Inorg. Chem. **2004**, *43*, 4203–4209

Synthesis, Structure, and Magnetic Properties of a [Mn22] Wheel-like Single-Molecule Magnet

Muralee Murugesu,[†] James Raftery,[‡] Wolfgang Wernsdorfer,[¶] George Christou,[†] and Euan K. Brechin*[,‡]

Department of Chemistry, The University of Manchester, Oxford Road, Manchester, M13 9PL, U.K., Department of Chemistry, University of Florida, Gainesville, Florida 32611-7200, and Laboratoire Louis Néel-CNRS, 38042 Grenoble, Cedex 9, France

Received March 22, 2004

The synthesis and magnetic properties of the compound $[Mn_{22}O_6(OMe)_{14}(O_2CMe)_{16}(tmp)_8(HIm)_2]$ **1** are reported. Complex **1** was prepared by treatment of $[Mn_3O(MeCO_2)_6(HIm)_3](MeCO_2)$ (HIm = imidazole) with 1,1,1-tris-(hydroxymethyl)propane (H_3tmp) in MeOH. Complex **1**·2MeOH crystallizes in the orthorhombic space group *Pbca*. The molecule consists of a metallic core of 2 Mn^{IV}, 18 Mn^{III}, and 2 Mn^{II} ions linked by a combination of 6 μ_3-bridging O^{2-} ions, 14 μ_3- and μ_2-bridging MeO^- ions, 16 μ-$MeCO_2^-$ ligands, and 8 tmp^{3-} ligands, which use their alkoxide arms to bridge in a variety of ways. The metal–oxygen core is best described as a wheel made from $[Mn_3O_4]$ partial cubes and $[Mn_3O]$ triangles. Variable-temperature direct current (dc) magnetic susceptibility data were collected for complex **1** in the 1.8–300 K temperature range in a 1 T applied field. The $\chi_M T$ value steadily decreases from 56 cm^3 K mol^{-1} at 300 K to 48.3 cm^3 K mol^{-1} at 30 K and then increases slightly to reach a maximum value of 48.6 cm^3 K mol^{-1} at 15 K before dropping rapidly to 40.3 cm^3 K mol^{-1} at 5 K. The ground-state spin of complex **1** was established by magnetization measurements in the 0.1–2.0 T and 1.80–4.00 K ranges. Fitting of the data by a matrix-diagonalization method to a model that assumes only the ground state is populated and incorporating only axial zero-field splitting ($D\hat{S}_z^2$), gave a best fit of $S = 10$, $g = 1.96$ and $D = -0.10$ cm^{-1}. The ac magnetization measurements performed on complex **1** in the 1.8–8 K range in a 3.5 G ac field oscillating at 50–1000 Hz showed frequency-dependent ac susceptibility signals below 3 K. Single-crystal hysteresis loop and relaxation measurements indicate loops whose coercivities are strongly temperature and time dependent, increasing with decreasing temperature and increasing field sweep rate, as expected for the superparamagnetic-like behavior of a single-molecule magnet, with a blocking temperature (T_B) of approximately 1.3 K.

Introduction

The search for large clusters of paramagnetic transition metal ions has been largely stimulated by the discovery of single-molecule magnetism.[1] This is the superparamagnetic-like behavior of molecules that combine a large spin ground state with a relatively large and negative easy-axis-type magnetoanisotropy, resulting in the observation of hysteresis in magnetization vs field studies. Manganese clusters are attractive candidates in this respect since they often display unusually large spin ground states and large *D* values, arising from the presence of Jahn−Teller distorted Mn^{III} ions.[2]

Examples of large clusters of 3d transition metal ions remain relatively uncommon, however, and those that contain more than 20 metals are extremely rare, confined to only a handful of clusters containing Cu,[3] Ni,[4] Co,[5] Fe,[6] and Mn.

* Author to whom correspondence should be addressed. E-mail: euan.k.brechin@man.ac.uk.
‡ The University of Manchester.
† University of Florida.
¶ Laboratoire Louis Néel-CNRS.

(1) (a) Sessoli, R.; Tsai, H.-L.; Schake, A. R.; Wang, S.; Vincent, J. B.; Folting, K.; Gatteschi, D.; Christou, G.; Hendrickson, D. N. *J. Am. Chem. Soc.* **1993**, *115*, 1804. (b) Sessoli, R.; Gatteschi, D.; Caneschi, A.; Novak, M. A. *Nature* **1993**, *365*, 141.
(2) Hendrickson, D. N.; Christou, G.; Ishimoto, H.; Yoo, J.; Brechin, E. K.; Yamaguchi, A.; Rumberger, E. M.; Aubin, S. M. J.; Sun, Z.; Aromí, G. *Polyhedron* **2001**, *20*, 1479.
(3) See for example: (a) Murugesu, M.; Anson, C. E.; Powell, A. K. *Chem. Commun*. **2002**, 1054. (b) Abedin, T. S. M.; Thompson, L. K.; Miller, D. O.; Krupicka, E. *Chem. Commun*. **2003**, 708.
(4) Dearden, A. L.; Parsons, S.; Winpenny, R. E. P. *Angew. Chem., Int. Ed*. **2001**, *40*, 151.
(5) Brechin, E. K.; Harris, S. G.; Harrison, A.; Parsons, S.; Whittaker, A. G.; Winpenny, R. E. P. *Chem. Commun*. **1997**, 653.

10.1021/ic049620h CCC: $27.50
Published on Web 06/12/2004

Scheme 1. Tripodal Ligands 1,1,1-Tris(hydroxymethyl)ethane (H_3thme), 1,1,1-Tris(hydroxymethyl)propane (H_3tmp), and Pentaerythritol (H_4peol)

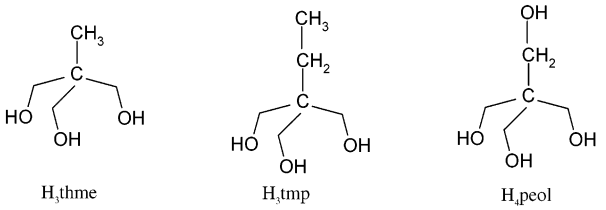

For Mn, these complexes include [Mn21],[7,8] [Mn26],[9] [Mn30],[10] and [Mn84],[11] and in each case, the manganese cluster has displayed single-molecule magnet (SMM) behavior.

Tripodal ligands, such as 1,1,1-tris(hydroxymethyl)ethane (H_3thme, Scheme 1), have been used extensively in the synthesis of oxovanadium and oxomolybdenum clusters.[12] Here, the disposition of the three alkoxide arms of the trianion directs the formation of triangular M_3 units, where each arm of the ligand bridges one edge of the triangle. These units are then combined to form complexes whose structures are commonly based on octahedra. We have previously reported the synthesis and magnetic properties of a number of Fe and Mn clusters built using tripodal ligands.[13] These ligands are excellent candidates for use in paramagnetic cluster synthesis as they have the ability to act as both terminal and bridging ligands depending on their degree of protonation: each alkoxide arm can potentially act as a μ_3-bridge.

In Mn chemistry, H_3thme has been employed in the synthesis of [Mn12],[14] [Mn10],[15] [Mn9],[16] [Mn8],[14] and [Mn6][17] clusters, and in each case, the tripodal ligand has formed M_3 triangular units: in [Mn9], the M_3 unit is 'isolated' but for [Mn12], [Mn8], and [Mn6] these units combine, producing rod-like structures consisting of 10, 6, and 4 edge-sharing triangles, respectively. In [Mn10], made under solvothermal reaction conditions, the thme^{3-} ligands act as μ_3-bridges, capping the triangular faces of a decametalate core. These compounds are almost exclusively obtained from the reactions of the Mn triangular species $[Mn_3O(RCO_2)_6(L)_3]^{0,+}$ with the tripodal ligand in solutions of MeCN. The introduction of alcohol to other systems has been shown previously to lead to either an increase in nuclearity and/or to the formation of new structural types with differing oxidation states.[18,13] We were, therefore, interested to see the effect of performing similar reactions in MeOH in order to extend the idea of alcoholysis as a route to new Mn clusters. In the present work, we describe the synthesis, structure, and magnetic properties of a new [Mn22] cluster made from the reaction of a Mn^{III} triangle with the tripodal ligand 1,1,1-tris(hydroxymethyl)propane (H_3tmp).

Experimental Section

Synthesis. All manipulations were performed under aerobic conditions, using materials as received. $[Mn_3O(MeCO_2)_6(HIm)_3](MeCO_2)$ (HIm = imidazole) was made as previously reported.[19]

$[Mn_{22}O_6(OMe)_{14}(O_2CMe)_{16}(tmp)_8(HIm)_2]$ (1). To a stirred red-brown solution of $[Mn_3O(MeCO_2)_6(HIm)_3](MeCO_2)$ (0.500 g) in MeOH (20 mL) was added solid H_3tmp (0.067 g). The mixture was stirred for 10 h, then filtered, and the solution was layered with diethyl ether (Et_2O). After 7 days the resulting black crystals of **1** were collected by filtration, washed with Et_2O, and dried in vacuo. The yield was approximately 15%. Anal. Calcd for $Mn_{22}C_{100}H_{186}O_{76}N_4$: C, 31.04; H, 4.85; N, 1.45; Mn, 31.24. Found: C, 31.51; H, 5.13; N, 1.78; Mn, 31.88.

X-ray Crystallography and Structure Solution. A crystal was mounted using a drop of fomblin (perfluoropolymethylisopropyl ether) oil in a Hamilton Cryoloop, and data were collected on a Bruker Smart Apex CCD diffractometer at 100 K using Mo radiation. The crystal structure was solved using SHELXS and refined by full-matrix least-squares with SHELXTL. Hydrogens were positioned geometrically and refined using the riding model. The asymmetric unit is a "half wheel", with the other half being generated by a crystallographic center of symmetry, and a methanol molecule. Crystallographic data and structure refinement details are listed in Table 1.

Other Measurements. Elemental analyses were performed by The University of Manchester Microanalysis Service. Variable-temperature, solid-state direct current (dc) magnetic susceptibility data down to 1.80 K were collected on a Quantum Design MPMS-XL SQUID magnetometer, equipped with a 7 T dc magnet at the University of Florida. Diamagnetic corrections were applied to the observed paramagnetic susceptibilities using Pascal's constants. The dc measurements below 1.80 K were performed on single crystals using an array of micro-SQUIDS.[20]

Results and Discussion

Synthesis. The reaction between the neutral triangular species $[Mn_3O(RCO_2)_6(L)_3]$ (where R = Me, Ph, $C(CH_3)_3$ and L = py) with the tripodal ligands H_3thme, H_3tmp, and H_4peol in MeCN has previously been shown to produce a

(6) Müller, A.; Sarkar, S.; Shah, S. Q. N.; Bögge, H.; Schmidtmann, M.; Sarkar, S.; Kögerler, P.; Haupfliesch, B.; Trautwein, A. X.; Schunemann, V. *Angew. Chem., Int. Ed.* **1999**, *38*, 3238.
(7) Brockman, J. T.; Huffman, J. C.; Christou, G. *Angew. Chem., Int. Ed.* **2002**, *114*, 2616.
(8) Sañudo, E. C.; Brechin, E. K.; Boskovic, C.; Wernsdorfer, W.; Yoo, J.; Yamaguchi, A.; Concolino, T. R.; Abboud, K. A.; Rheingold, A. L.; Ishimoto, H.; Hendrickson, D. N.; Christou, G. *Polyhedron* **2003**, *23*, 2267.
(9) Jones, L. F.; Brechin, E. K.; Collison, D.; Harrison, A.; Teat, S. J.; Wernsdorfer, W. *Chem. Commun.* **2002**, 2974.
(10) (a) Soler, M.; Rumberger, E.; Folting, K.; Hendrickson, D. N.; Christou, G. *Polyhedron* **2001**, *20*, 1365. (b) Soler, M.; Wernsdorfer, W.; Folting, K.; Pink, M.; Christou, G. *J. Am. Chem. Soc.* **2004**, *126*, 2156.
(11) Tasiopoulos, A. J.; Vinslava, A.; Wernsdorfer, W.; Abboud, K. A.; Christou, G. *Angew. Chem., Int. Ed.* **2004**, *16*, 2117.
(12) Khan, M. I.; Zubieta, J. *Prog. Inorg. Chem.* **1995**, *43*, 1.
(13) (a) Brechin, E. K.; Soler, M.; Christou, G.; Davidson, J.; Hendrickson, D. N.; Parsons, S.; Wernsdorfer, W. *Polyhedron* **2003**, *22*, 1771. (b) Jones, L. F.; Batsanov, A.; Brechin, E. K.; Collison, D.; Helliwell, M.; Mallah, T.; McInnes, E. J. L.; Piligkos, S. *Angew. Chem., Int. Ed.* **2002**, *41*, 4318.
(14) Brechin, E. K.; Soler, M.; Christou, G.; Helliwell, M.; Teat, S. J.; Wernsdorfer, W. *Chem. Commun.* **2003**, 1276.
(15) Cavaluzzo, M.; Chen, Q.; Zubieta, J. *J. Chem. Soc., Chem. Commun.* **1993**, 131.
(16) Brechin, E. K.; Soler, M.; Davidson, J.; Hendrickson, D. N.; Parsons, S.; Christou, G. *Chem. Commun.* **2002**, 2252.
(17) Brechin, E. K.; Murugesu, M.; Muryn, C.; Christou, G. Unpublished results.
(18) Cañada-Vilalta, C.; Pink, M.; Christou, G. *Chem. Commun.* **2003**, 1240.
(19) Vincent, J. B.; Chang, H.-R.; Folting, K.; Huffman, J. C.; Christou, G.; Hendrickson, D. N. *J. Am. Chem. Soc.* **1987**, *109*, 5703.
(20) Wernsdorfer, W. *Adv. Chem. Phys.* **2001**, *118*, 99.

Table 1. Crystallographic Data for Complex **1**

	1
formula[a]	$C_{102}H_{192}Mn_{22}N_4O_{78}$
fw (g mol^{-1})	3931.28
space group	*Pbca*
a (Å)	25.229(13)
b (Å)	20.655(10)
c (Å)	33.560(16)
α (deg)	90
β (deg)	90
γ (deg)	90
V (Å^3)	17488(15)
Z	4
ρ_{calcd} (g cm^{-3})	1.493
T (K)	100(2)
λ (Å)[b]	0.71073
μ (mm^{-1})	1.609
R (*R*$_w$) (%)[c]	8.19 (27.47)

[a] Including solvate molecules. [b] Graphite monochromator. [c] $R = \sum||F_o| - |F_c||/\sum|F_o|$; wR2 = $[\sum[w(F_o^2 - F_c^2)^2]/\sum[w(F_o^2)^2]]^{1/2}$, where $w = 1/[\sigma^2(F_o^2) + (0.0991p)^2]$ and $p = [\max(F_o^2,0) + 2F_c^2]/3$.

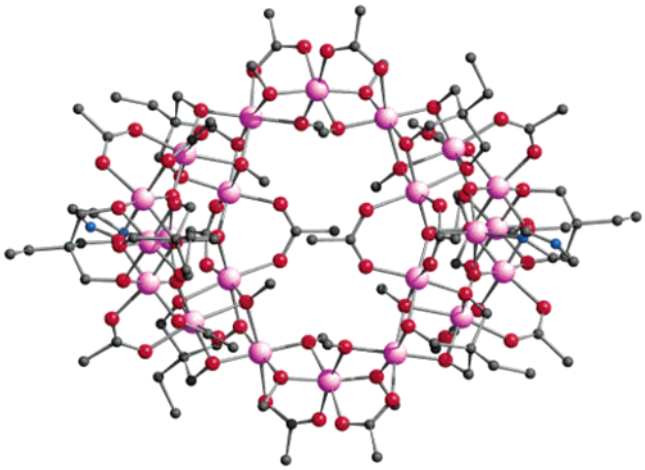

Figure 1. Structure of **1** in the crystal.

number of large Mn clusters, but the equivalent reactions with the all Mn^{III} triangular species $[Mn_3O(RCO_2)_6(L)_3](X)$ (X = ClO_4^-, etc) has, thus far, proved unsuccessful. For example, the enneanuclear species $[Mn_9O_7(RCO_2)_{11}(tripod)_1(py)_3(H_2O)_2]$ (with R = Me and tripod = H_3thme, H_3tmp, Hpeol; and for R = Ph, $C(CH_3)_3$ with tripod = Hpeol),[16] the dodecametallic cluster $[Mn_{12}O_4(OH)_2(PhCO_2)_{12}(thme)_4(py)_2]$,[14] and the octametallic cluster $[Mn_8O_4(C(CH_3)_3)_{10}(thme)_2(py)_2]$[14] can all be isolated from the simple 1:1 reaction of neutral Mn triangles with tripods in MeCN. Which cluster is isolated is dependent upon both the identity of the tripod and the carboxylate. When the identical reactions are performed using the ClO_4^- salts of the triangles, no isolable products are obtained. Complex **1** results from our first attempts to perform similar reactions in MeOH. Reaction of the Mn^{III} metal triangle $[Mn_3O(MeCO_2)_6(HIm)_3](MeCO_2)$ (HIm = imidazole) with 1 equiv of 1,1,1-tris(hydroxymethyl)propane (H_3tmp) in MeOH, followed by diffusion of diethyl ether (Et_2O) into the solution, affords the mixed-valent species $[Mn^{IV}_2Mn^{III}_{18}Mn^{II}_2O_6(OMe)_{14}(O_2CMe)_{16}(tmp)_8(HIm)_2]$ **1** in good yield after 1 week.

Description of Crystal Structure. Complex **1** (Figure 1, selected bond lengths and angles are given in Tables 2 and 3, respectively) crystallizes in the orthorhombic space group *Pbca*. The core of **1** (Figure 2) can be described as a central $[Mn_{16}O_{30}]$ "wheel" (containing Mn1, Mn2, Mn3, Mn6, Mn7, Mn8, Mn9, Mn10, and symmetry equivalents), with a $[Mn_3O_4]$ partial cube (missing one vertex, Mn4, Mn5, Mn11, O7, O8, O9, O34, and symmetry equivalents) attached on each side, one above and one below the 'plane' of the wheel (Figure 3). The two "sides" of this $[Mn_{16}O_{30}]$ wheel each comprise two $[Mn_3O_4]$ partial cubes, each missing one vertex (e.g. Mn3, Mn7, Mn8, O1, O2, O3, O33) and two $[Mn_3O]$ triangles (e.g. Mn8, Mn1, Mn10, O36 and Mn10, O38, O37, O36) which share an Mn−O "arm". The two sides of the wheel are joined together via Mn9. Within the $[Mn_{16}O_{30}]$ wheel, the central 10 Mn ions (Mn1, Mn6, Mn7, Mn8, Mn9) are approximately planar, forming an "inner" [Mn10] wheel with Mn2, Mn3, and Mn10 (and symmetry equivalents) lying above and below this plane, respectively. The Mn ions in the $[Mn_{16}O_{30}]$ wheel are all six-coordinate Mn^{III} ions in Jahn−Teller distorted octahedral geometries, with one exception: Mn10 (and symmetry equivalent) is a tetrahedral Mn^{II} ion. The peripheral $[Mn_3O_4]$ partial cubes contain one Mn^{IV} ion (Mn11) and two Mn^{III} (Mn4, Mn5) ions. The Mn−O−Mn angles within these units are in the range 113.2−122.8°. Within the partial cubes, the angles range from 92.1 to 99.0° for the μ_3-O atoms and from 101.8 to 108.6° for the μ_2-O atoms.

The six O^{2-} ions are found in the $[Mn_{16}O_{30}]$ wheel, all attached to Mn10, adopting their usual μ_3-bridging mode. Two of the oxides (O37, O38) link the $[Mn_{16}O_{30}]$ wheel to the peripheral $[Mn_3O_4]$ units. The MeO^- ligands are of two types: eight bridge in a μ_2-fashion between the Mn ions in

Table 2. Selected Interatomic Distances (Å) for **1**

Mn1−O36	1.850(7)	Mn4−O37	1.825(7)	Mn3−O18	2.072(8)	Mn6−O35	2.129(7)
Mn1−O12	1.971(7)	Mn4−O7	1.925(7)	Mn3−O33	2.213(8)	Mn6−O11	2.152(8)
Mn1−O25	2.013(8)	Mn4−O23	2.035(8)	Mn7−O29	1.898(8)	Mn9−O29	1.983(8)
Mn1−O35	2.022(7)	Mn4−O9	2.043(8)	Mn7−O3	1.925(8)	Mn9−O10	1.983(8)
Mn1−O20	2.117(8)	Mn4−O16	2.046(8)	Mn7−O33	1.962(8)	Mn9−O32	2.136(7)
Mn1−O14	2.161(8)	Mn4−O34	2.138(8)	Mn7−O28	1.985(8)	Mn9−O27	2.172(8)
Mn2−O37	1.836(7)	Mn5−O38	1.843(7)	Mn7−O1	2.100(8)	Mn10−O36	2.081(7)
Mn2−O14	1.938(7)	Mn5−O8	1.925(7)	Mn7−O30	2.146(8)	Mn10−O37	2.097(7)
Mn2−O13	1.968(7)	Mn5−O9	1.968(8)	Mn8−O36	1.852(7)	Mn10−O38	2.102(7)
Mn2−O24	1.985(8)	Mn5−O22	1.983(9)	Mn8−O1	1.930(7)	Mn10−N1	2.134(9)
Mn2−O15	2.124(8)	Mn5−O17	2.139(8)	Mn8−O2	1.984(8)	Mn11−O6	1.839(8)
Mn2−O35	2.242(8)	Mn5−O34	2.232(7)	Mn8−O19	1.990(8)	Mn11−O4	1.841(8)
Mn3−O38	1.824(7)	Mn6−O32	1.881(8)	Mn8−O26	2.107(8)	Mn11−O5	1.880(9)
Mn3−O3	1.959(7)	Mn6−O13	1.907(7)	Mn8−O33	2.219(7)	Mn11−O34	1.987(7)
Mn3−O21	2.000(8)	Mn6−O31	1.988(8)	Mn9−O30	1.857(8)	Mn11−O8	2.017(7)
Mn3−O2	2.003(7)	Mn6−O12	1.992(7)	Mn9−O31	1.892(8)	Mn11−O7	2.042(8)

Table 3. Selected Interatomic Angles (deg) for **1**

O36−Mn1−O12	171.7(3)	O37−Mn4−O34	94.7(3)	O36−Mn8−O19	94.0(3)
O36−Mn1−O25	95.3(3)	O7−Mn4−O34	77.7(3)	O1−Mn8−O19	90.1(3)
O12−Mn1−O25	91.4(3)	O23−Mn4−O34	92.1(3)	O2−Mn8−O19	169.0(3)
O36−Mn1−O35	92.9(3)	O9−Mn4−O34	81.5(3)	O36−Mn8−O26	93.6(3)
O12−Mn1−O35	79.7(3)	O16−Mn4−O34	166.7(3)	O1−Mn8−O26	89.2(3)
O25−Mn1−O35	167.9(3)	O38−Mn5−O8	169.3(3)	O2−Mn8−O26	97.2(3)
O36−Mn1−O20	94.1(3)	O38−Mn5−O9	92.0(3)	O19−Mn8−O26	93.6(3)
O12−Mn1−O20	90.3(3)	O8−Mn5−O9	87.7(3)	O36−Mn8−O33	99.0(3)
O25−Mn1−O20	93.0(3)	O38−Mn5−O22	93.2(3)	O1−Mn8−O33	77.9(3)
O35−Mn1−O20	95.2(3)	O8−Mn5−O22	86.1(3)	O2−Mn8−O33	78.8(3)
O36−Mn1−O14	90.0(3)	O9−Mn5−O22	171.8(3)	O19−Mn8−O33	90.2(3)
O12−Mn1−O14	85.2(3)	O38−Mn5−O17	98.5(3)	O26−Mn8−O33	166.5(3)
O25−Mn1−O14	90.4(3)	O8−Mn5−O17	92.2(3)	O30−Mn9−O31	171.3(3)
O35−Mn1−O14	80.8(3)	O9−Mn5−O17	94.0(3)	O30−Mn9−O29	80.7(3)
O20−Mn1−O14	174.5(3)	O22−Mn5−O17	91.6(4)	O31−Mn9−O29	93.7(3)
		O38−Mn5−O34	92.1(3)	O30−Mn9−O10	94.1(3)
O37−Mn2−O14	89.5(3)	O8−Mn5−O34	77.2(3)	O31−Mn9−O10	92.3(3)
O37−Mn2−O13	176.4(3)	O9−Mn5−O34	80.8(3)	O29−Mn9−O10	171.2(3)
O14−Mn2−O13	88.9(3)	O22−Mn5−O34	92.6(3)	O30−Mn9−O32	97.1(3)
O37−Mn2−O24	92.0(3)	O17−Mn5−O34	168.3(3)	O31−Mn9−O32	76.9(3)
O14−Mn2−O24	165.8(3)	O32−Mn6−O13	172.5(3)	O29−Mn9−O32	96.8(3)
O13−Mn2−O24	88.8(3)	O32−Mn6−O31	80.9(3)	O10−Mn9−O32	90.8(3)
O37−Mn2−O15	95.4(3)	O13−Mn6−O31	92.5(3)	O30−Mn9−O27	90.7(3)
O14−Mn2−O15	95.9(3)	O32−Mn6−O12	98.3(3)	O31−Mn9−O27	95.7(3)
O13−Mn2−O15	88.0(3)	O13−Mn6−O12	88.2(3)	O29−Mn9−O27	87.7(3)
O24−Mn2−O15	98.0(3)	O31−Mn6−O12	179.0(3)	O10−Mn9−O27	85.4(3)
O37−Mn2−O35	99.1(3)	O32−Mn6−O35	96.4(3)	O32−Mn9−O27	171.6(3)
O14−Mn2−O35	80.6(3)	O13−Mn6−O35	81.6(3)	O36−Mn10−O37	103.1(3)
O13−Mn2−O35	77.4(3)	O31−Mn6−O35	102.8(3)	O36−Mn10−O38	105.7(3)
O24−Mn2−O35	85.2(3)	O12−Mn6−O35	76.7(3)	O37−Mn10−O38	99.9(3)
O15−Mn2−O35	165.0(3)	O32−Mn6−O11	90.7(3)	O36−Mn10−N1	114.5(3)
O38−Mn3−O3	174.8(3)	O13−Mn6−O11	92.4(3)	O37−Mn10−N1	121.5(3)
O38−Mn3−O21	93.3(3)	O31−Mn6−O11	86.7(3)	O38−Mn10−N1	110.2(3)
O3−Mn3−O21	88.8(3)	O12−Mn6−O11	93.9(3)		
O38−Mn3−O2	89.1(3)	O35−Mn6−O11	168.9(3)	O6−Mn11−O4	93.3(4)
O3−Mn3−O2	87.8(3)			O6−Mn11−O5	93.0(4)
O21−Mn3−O2	165.8(3)	O29−Mn7−O3	173.0(3)	O4−Mn11−O5	92.6(4)
O38−Mn3−O18	97.3(3)	O29−Mn7−O33	95.0(3)	O6−Mn11−O34	171.1(4)
O3−Mn3−O18	87.3(3)	O3−Mn7−O33	83.0(3)	O4−Mn11−O34	91.4(3)
O21−Mn3−O18	92.8(4)	O29−Mn7−O28	92.3(3)	O5−Mn11−O34	94.3(3)
O2−Mn3−O18	100.8(3)	O3−Mn7−O28	90.4(3)	O6−Mn11−O8	94.0(3)
O38−Mn3−O33	99.4(3)	O33−Mn7−O28	170.4(4)	O4−Mn11−O8	172.4(3)
O3−Mn3−O33	76.0(3)	O29−Mn7−O1	98.6(3)	O5−Mn11−O8	89.1(3)
O21−Mn3−O33	87.3(3)	O3−Mn7−O1	87.7(3)	O34−Mn11−O8	81.2(3)
O2−Mn3−O33	78.6(3)	O33−Mn7−O1	80.1(3)	O6−Mn11−O7	93.5(3)
O18−Mn3−O33	163.3(3)	O28−Mn7−O1	92.7(3)	O4−Mn11−O7	92.4(3)
O37−Mn4−O7	172.3(3)	O29−Mn7−O30	75.6(3)	O5−Mn11−O7	171.5(3)
O37−Mn4−O23	93.4(3)	O3−Mn7−O30	97.9(3)	O34−Mn11−O7	78.7(3)
O7−Mn4−O23	85.6(3)	O33−Mn7−O30	96.7(3)	O8−Mn11−O7	85.0(3)
O37−Mn4−O9	91.9(3)	O28−Mn7−O30	91.1(3)		
O7−Mn4−O9	88.4(3)	O1−Mn7−O30	173.2(3)		
O23−Mn4−O9	172.1(3)	O36−Mn8−O1	174.9(3)		
O37−Mn4−O16	96.9(3)	O36−Mn8−O2	87.5(3)		
O7−Mn4−O16	90.8(3)	O1−Mn8−O2	87.9(3)		
O23−Mn4−O16	93.7(3)				
O9−Mn4−O16	91.6(3)				

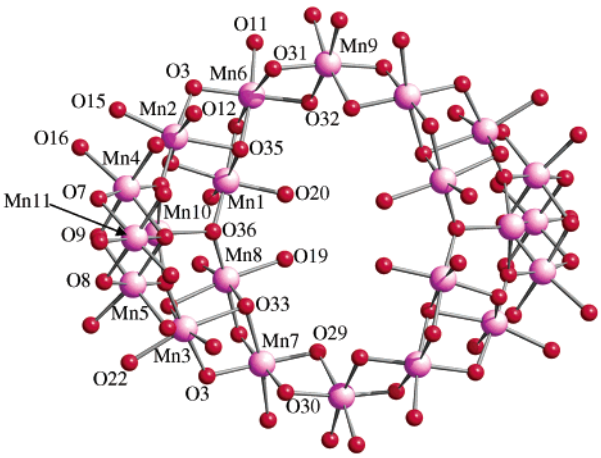

Figure 2. Metal−oxygen core in **1**, viewed from above the central wheel.

the "inner" [Mn_{10}] wheel; the remaining six are all μ_3-bridging, four within the [$Mn_{16}O_{30}$] wheel (e.g., O33, O35) and two in the peripheral [Mn_3O_4] partial cubes (O34). The eight tmp^{3-} ligands fall into two categories: six use each arm in a μ_2-fashion, four of which form the corners of the [Mn_3O_4] partial cubes in the [$Mn_{16}O_{30}$] wheel while two form the corners in the peripheral [Mn_3O_4] partial cubes; the remaining two tmp^{3-} ligands chelate [Mn11] in the peripheral partial cube, each arm (O4, O5, O6) binding in a terminal fashion with bond lengths in the range 1.839−1.880 Å, and each is also hydrogen-bonded to either a MeOH solvent molecule (e.g., O5−O39, 2.860 Å) or an imidazole on a neighboring molecule. The 16 $MeCO_2^-$ ligands all bond in the expected μ-mode, and the two HIm ligands bond terminally to the tetrahedral Mn^{II} ion (Mn10). The protonated N atom of the HIm ligands H-bond to $CH_3CO_2^-$ and tmp^{3-} ligands on neighboring molecules (e.g., N2−O4, 2.882 Å; N2−O7, 2.925 Å) as do the MeOH solvent molecules, forming a serpentine-like or zigzag packing of [Mn22] molecules in the crystal (Figure 4).

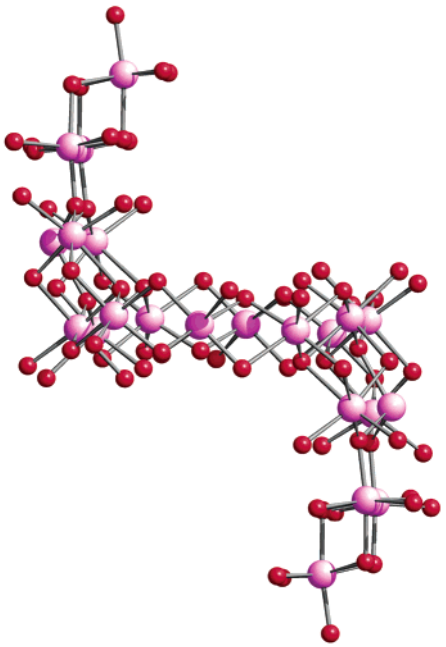

Figure 3. Metal−oxygen core in **1**, viewed from the side of the central wheel.

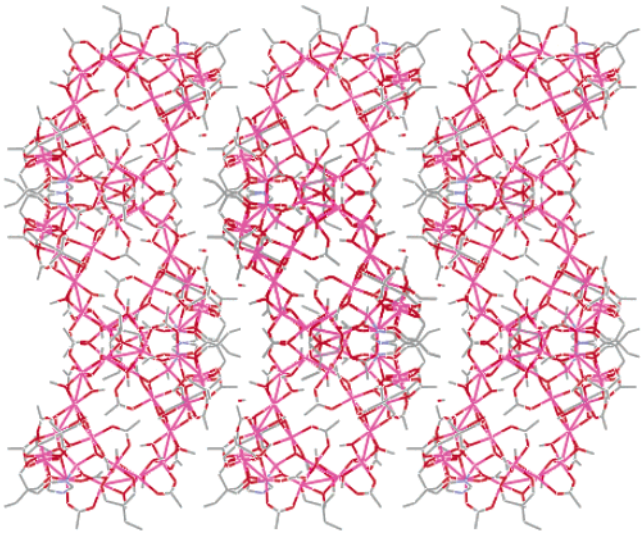

Figure 4. Packing of **1** in the crystal.

The cavity within the central wheel is oval shaped with metal−metal distances ranging from ∼11 Å (Mn9−Mn9A) to ∼9 Å (Mn8−Mn8A). All oxidation states were assigned using a combination of bond lengths, charge balance considerations, and bond valence sum (BVS) calculations (Table 4).[21] All the Mn^{III} ions show the expected Jahn−Teller elongations, although the elongation axes are not all parallel.

Magnetic Susceptibility Studies. The magnetic properties of complex **1** were investigated by solid-state magnetic susceptibility (χ_M) measurements in the 1.8 to 300 K temperature range and in a dc field of 1 T (Figure 5). The room temperature $\chi_M T$ value of approximately 56 cm^3 K mol^{-1} is slightly lower than the expected value for a unit containing 2 Mn^{IV}, 18 Mn^{III}, and 2 Mn^{II} ions (∼66 cm^3 K mol^{-1}). The $\chi_M T$ value steadily decreases from 56 cm^3 K mol^{-1} at 300 K to 48.3 cm^3 K mol^{-1} at 30 K and then slightly increases to reach a maximum value of 48.6 cm^3 K mol^{-1} at 15 K before dropping rapidly to 40.3 cm^3 K mol^{-1} at 5 K (Figure 5). The dramatic decrease of the $\chi_M T$ value at low temperature may be a consequence of Zeeman effects from the dc field and/or the presence of intermolecular antiferromagnetic interactions between clusters. The data strongly suggest predominantly antiferromagnetic exchange interactions within the cluster with a non-zero spin ground state, and the 15 K value indicates an approximately $S = 10$ spin ground state.

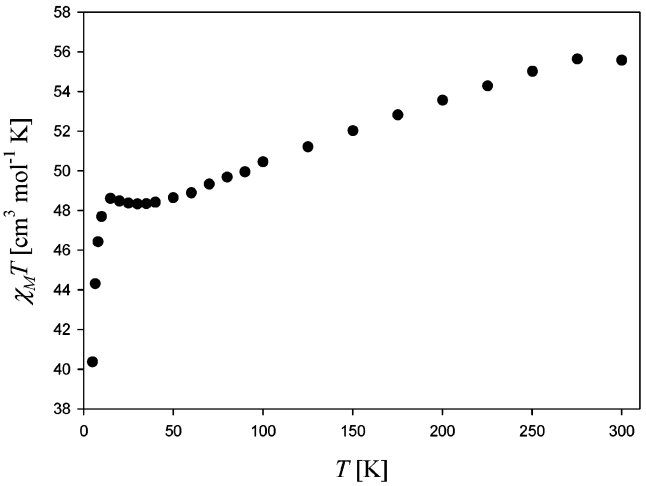

Figure 5. Plot of $\chi_M T$ vs T for **1** in the 1.8−300 K temperature range in a field of 1 T.

Table 4. Bond Valence Sum Calculations for **1**

atom	Mn(II)	Mn(III)	Mn(IV)	atom	Mn(II)	Mn(III)	Mn(IV)
Mn1	3.108	2.843	2.983	Mn7	3.247	2.971	3.118
Mn2	3.236	2.960	3.109	Mn8	3.217	2.944	3.092
Mn3	3.234	2.959	3.106	Mn9	3.299	3.016	3.168
Mn4	3.286	3.006	3.155	Mn10	1.605	1.468	1.539
Mn5	3.239	2.962	3.109	Mn11	3.894	3.562	3.739
Mn6	3.225	2.951	3.098				

To determine the spin ground-state value for complex **1**, magnetization measurements were carried out in the range 1.8−4 K and between 0.1 and 2 T (0.1, 0.5, 1, and 2 T). The data were fit by a matrix-diagonalization method (using the program MAGNET[22]) to a model that assumes only the ground state is populated, includes axial zero-field splitting ($D\hat{S}_z^2$), and carries out a full powder average. The data are plotted as reduced magnetization $M/(N\mu_B)$ versus H/T in Figure 6. The best fit gave $S = 10$, $g = 1.96$, and $D = -0.10$ cm^{-1}. When fields up to 7 T were employed, a poorer-quality fit was obtained. This behavior is characteristic of low-lying excited states with S values greater than the ground state of $S = 10$. Low-lying excited states are a common problem in large clusters, particularly when there are Mn^{II} ions present, as in this system, since these give weak exchange interactions. The result of this is that population of excited states will be difficult to avoid even at very low temperatures.

(21) (a) Brown, I. D.; Altermatt, D. *Acta Crystallogr., Sect. B* **1985**, *41*, 244. (b) Zhang, X. Y.; O'Connor, C. J.; Jameson, G. B.; Pope, M. T. *Inorg. Chem.* **1996**, *35*, 30. (c) Thorp, H. H. *Inorg. Chem.* **1992**, *31*, 1585.

(22) Davidson, E. R. *MAGNET*; Indiana University: Bloomington, IN.

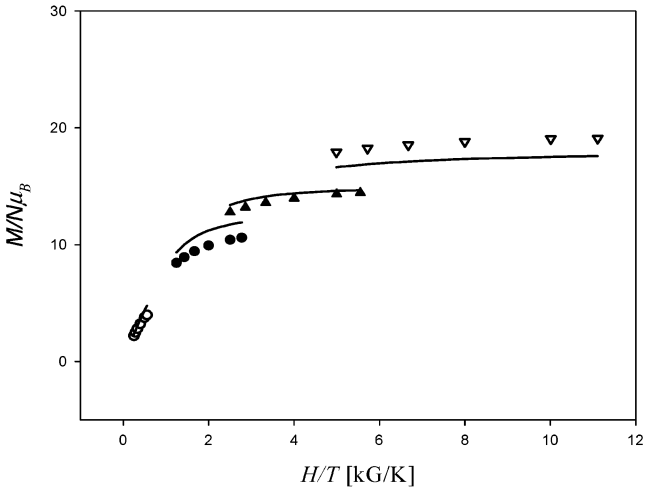

Figure 6. Plot of reduced magnetization vs H/T for **1**. The solid lines are the fit of the data to an $S = 10$ state, with $D = -0.10$ cm^{-1} and $g = 1.96$.

Because the fitting procedure assumes only the ground state is populated at low temperatures, the use of data collected at higher fields tends to overestimate the value of S, and consequently, the use of only low-field data in the fits helps to avoid this problem and provide more reliable results.

The S and D values obtained for **1** suggest an upper limit to the potential energy barrier (U) to magnetization reversal of $U = S^2|D| = 10$ cm^{-1} = 14 K. This suggests that complex **1** may exhibit SMM behavior.

Ac magnetization measurements were performed on complex **1** in the 1.8−8 K range in a 3.5 G ac field, oscillating at 50−1000 Hz (Figure 7). Frequency-dependent out-of-phase ac susceptibility signals were seen below approximately 3 K (but no peaks are observed), along with a concomitant decrease in the in-phase signal. The magnitude of the in-phase $\chi'_M T$ vs T signals at >3 K supports the aforementioned spin ground state.

Single-Crystal Hysteresis Measurements. Single-crystal hysteresis loop and relaxation measurements were performed using a micro-SQUID setup.[20] Preliminary studies of magnetization performed at very low temperature and high fields show that complex **1** behaves as an SMM with long relaxation times. Figure 8 presents typical magnetization (M) vs applied dc field measurements at a field sweep rate of 0.07 T/s. A hysteresis loop was observed, whose coercivity was strongly temperature and time dependent, increasing with decreasing temperature and increasing field sweep rate, as expected for the superparamagnetic-like behavior of an SMM. The blocking temperature (T_B) is ∼1.3 K. Above this temperature, there is no hysteresis; i.e., the spin relaxes faster to equilibrium than the time scale of the hysteresis loop measurement. The hysteresis loops do not show the step-like features indicative of resonant quantum tunneling of magnetization between the energy states of the molecule. This absence can be rationalized as being primarily due to a distribution of molecular environments and, thus, a distribution of magnetization relaxation barriers. In addition, weak intermolecular interactions (exchange and/or dipolar) and low-lying excited states will also contribute to broadening of steps.[8−11]

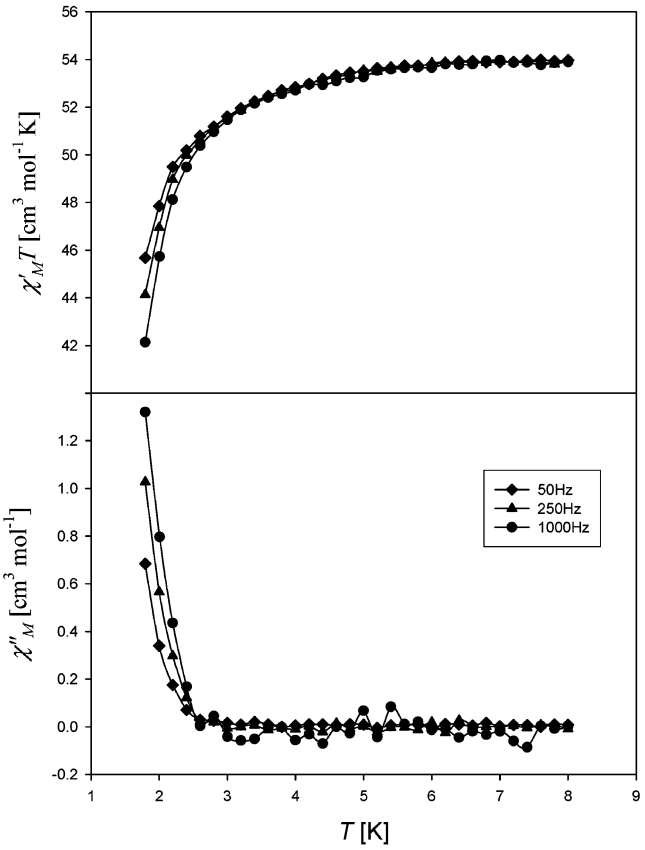

Figure 7. Plots of the in-phase (χ_M') signal as $\chi_M' T$ and out-of-phase (χ_M'') signal in ac susceptibility studies vs temperature in a 3.5 G field, oscillating at the indicated frequencies.

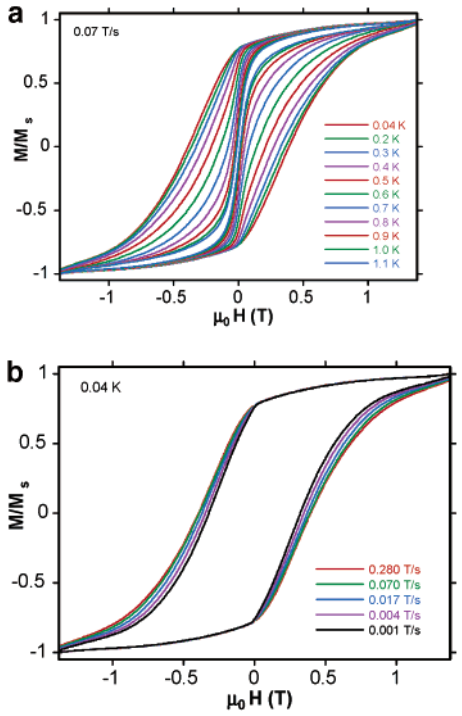

Figure 8. Magnetization (M) vs dc field hysteresis loops for **1**: (a) at a field scan rate of 0.07 T/s in the temperature range 1.1−0.04 K; (b) at a temperature of 0.04 K and in the field scan rates 0.280−0.01 T/s.

In Figure 9, we plot several isothermal relaxations of the magnetization as a function of time. The procedure used to obtain these curves was the following: first, a strong field

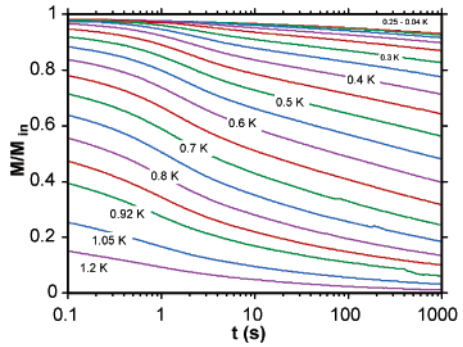

Figure 9. Single-crystal relaxation measurements of **1** plotted as M/M_{in}-vs-t curves. All data were normalized by the initial magnetization M_{in} at 0.04 K.

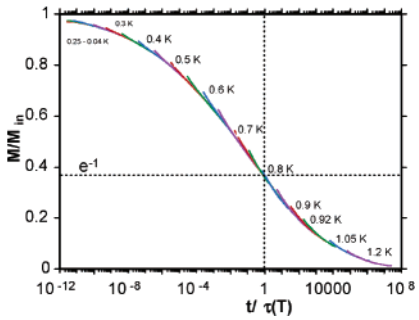

Figure 10. Single-crystal relaxtion measurements of **1**: scaling plot of $M(t)$ vs t/τ (T).

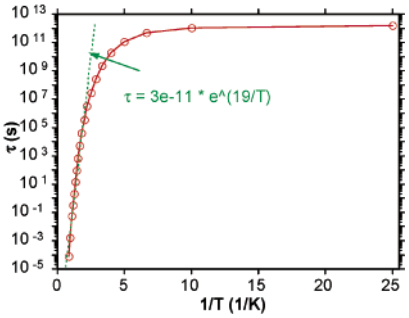

Figure 11. Arrhenius plot of the relaxation rate for **1** plotted as τ(s) vs $1/T$.

was applied at approximately 5 K in order to saturate the magnetization M to M_s, the temperature was lowered to a selected value, and then the external field was suddenly set to zero. This defined the time $t = 0$ s, and M was measured as a function of time. The relaxation of crystals of SMMs is often very complicated, leading to nonexponential relaxation laws, and we can notice that the M/M_{in}-vs-t curves of Figure 9 cannot be fitted by a simple law such as exponential, stretched exponential, square root, etc. To extract the temperature dependence of the mean relaxation time $\tau(T)$, we used a single scaling function $f(t/\tau(T))$.[23] The master function $f(x)$ is such that $f(t = 0) = M_{in}$ and $f(t = \infty) = 0$. All the data points of the relaxation measurements between 0.04 and 1.2 K and between $t = 2$ and 1000 s are scaled on a single master curve, using the transformation $t/\tau(T)$. This leads to the scaling plot of $M(t)$ vs $t/\tau(T)$, shown in Figure 10. Note that, thanks to this scaling analysis, $\tau(T)$ is determined without making any particular assumption about the relaxation law. This scaling analysis allows us to extract the mean relaxation time $\tau(T)$, which is shown in Figure 11 in an Arrhenius plot. Above approximately 0.3 K, the relaxation rate is temperature dependent. The straight line in Figure 11 is a fit to the Arrhenius law, yielding the values $\tau_0 = 3 \times 10^{-11}$ s and $U_{eff} = 19$ K. Below approximately 0.3 K, the relaxation rate becomes temperature independent, suggesting the presence of quantum tunneling of magnetization in the ground state.

Conclusions

Complex **1** represents the first example of a 3d transition metal cluster containing 22 metal centers and the fourth largest reported Mn cluster, behind [Mn26], [Mn30], and [Mn84]. The metal topology is unusual in Mn cluster chemistry and demonstrates the huge potential of both tripodal ligands and alcoholysis in cluster synthesis. Complex **1** is also a welcome new addition to the family of high-spin molecules and SMMs made with tripodal bridging ligands.

Acknowledgment. The authors acknowledge the EPSRC (UK) and the NSF for funding.

Supporting Information Available: An X-ray crystallographic file in CIF format is available for complex **1**. This material is available free of charge via the Internet at http://pubs.acs.org.

IC049620H

(23) (a) Thomas, L.; Caneschi, A.; Barbara, B. *Phys. Rev. Lett.* **1999**, *83*, 2398. (b) Affronte, M.; Lasjounias, J. C.; Wernsdorfer, W.; Sessoli, R.; Gatesschi, D.; Heath, S. L.; Fort, A.; Rettori, A. *Phys. Rev. B: Condens. Matter Mater. Phys.* **2002**, *66*, 064408.